

Detecting Parkinsonian Tremor from IMU Data Collected In-The-Wild using Deep Multiple-Instance Learning

Alexandros Papadopoulos¹, *Student Member, IEEE*, Konstantinos Kyritsis¹, *Student Member, IEEE*, Lisa Klingelhofer², Sevasti Bostanjopoulou³, K. Ray Chaudhuri⁴, Anastasios Delopoulos¹, *Member, IEEE*,

Abstract—Parkinson’s Disease (PD) is a slowly evolving neurological disease that affects about 1% of the population above 60 years old, causing symptoms that are subtle at first, but whose intensity increases as the disease progresses. Automated detection of these symptoms could offer clues as to the early onset of the disease, thus improving the expected clinical outcomes of the patients via appropriately targeted interventions. This potential has led many researchers to develop methods that use widely available sensors to measure and quantify the presence of PD symptoms such as tremor, rigidity and bradykinesia. However, most of these approaches operate under controlled settings, such as in lab or at home, thus limiting their applicability under free-living conditions. In this work, we present a method for automatically identifying tremorous episodes related to PD, based on IMU signals captured via a smartphone device. We propose a *Multiple-Instance Learning* approach, wherein a subject is represented as an unordered bag of accelerometer signal segments and a single, expert-provided, tremor annotation. Our method combines deep feature learning with a learnable pooling stage that is able to identify key instances within the subject bag, while still being trainable end-to-end. We validate our algorithm on a newly introduced dataset of 45 subjects, containing accelerometer signals collected entirely in-the-wild. The good classification performance obtained in the conducted experiments suggests that the proposed method can efficiently navigate the noisy environment of in-the-wild recordings.

I. INTRODUCTION

PARKINSON’S Disease is a long-term neurodegenerative condition that targets the central nervous system. Its symptomatology includes motor symptoms, such as tremor, bradykinesia, rigidity and hypomimia, as well as symptoms of non-motor nature like constipation and insomnia. In particular, tremor, bradykinesia and rigidity have been characterized as cardinal symptoms, in the sense that regardless of the symptom variability across different cases, the co-occurrence of at least two of these symptoms is a good indicator of the disease [1].

Despite being incurable, early diagnosis of PD holds much clinical benefit, since symptoms in earlier stages can be

managed more efficiently through appropriately targeted interventions [2]. However, the initial symptom onset can be so subtle that it goes unnoticed by the subjects until the disease has already progressed. Therefore, development of automated tools and methods that can observe and quantify the severity of PD symptoms outside laboratory conditions is a very useful research direction.

Following this line of research, many methods to automatically detect PD symptoms using data captured from a variety of sensors have been proposed. For instance, [3] and [4] use microphone-recorded speech signals to estimate the severity of speech impairment that exhibits in some PD patients using pre-computed features and Random Forest classifiers, while [5] proposes a CNN-based deep learning architecture that uses different CNN modules on different sets of features and then merges the learned representations. In a similar vein, the work of [6] uses a physical keyboard as a capturing device and proposes a method to transform the recorded sequence of key taps to a PD motor index. This approach is further refined by [7] who use the virtual keyboard from a smartphone and correlate the resulting index with the severity of bradykinesia and rigidity. Hand dexterity is also used as a means of PD diagnosis by the work of [8], who capture handwritten dynamics via a smart pen sensor and use it to train a CNN model to differentiate healthy from PD subjects. Many works employ *Inertial Measurement Unit (IMU)* sensors for data capturing. For example, [9] examines the feasibility of using body-worn IMU sensors for performing gait analysis, with the ultimate goal of inferring whether the wearer is a PD patient. In a similar spirit, [10] [11] and [12] make use of stand-alone accelerometer and gyroscope sensors to quantify tremor severity, while [13] explores the potential of using the IMU sensors embedded in smartphones as a viable means of monitoring and detecting tremor.

The idea of using sensors embedded in commercial off-the-self devices, such as smartphones and smartwatches is widely explored by *i-PROGNOSIS* [14], a European Horizon 2020 research programme that adopts a holistic approach towards early Parkinson’s diagnosis. In particular, it utilizes a multi-modal approach, where data are collected unobtrusively and in-the-wild, through smartphone embedded sensors including IMU, microphone and virtual keyboard, and consequently mapped to PD symptom indicators using machine learning techniques. Thus, rather than inferring the presence of PD from single symptom clues, *i-PROGNOSIS* examines the user’s

¹Multimedia Understanding Group, Information Processing Laboratory, Dept. of Electrical and Computer Engineering, Aristotle University of Thessaloniki, Greece ²Department of Neurology, Technical University of Dresden, Dresden, Germany ³Third Neurological Clinic, Papanikolaou Hospital, Thessaloniki, Greece ⁴International Parkinson Excellence Research Centre, King’s College Hospital NHS Foundation Trust, London, UK ⁵ Copyright 2019 IEEE. Personal use of this material is permitted. Permission from IEEE must be obtained for all other uses, in any current or future media, including reprinting/republishing this material for advertising or promotional purposes, creating new collective works, for resale or redistribution to servers or lists, or reuse of any copyrighted component of this work in other works

status with respect to multiple symptoms, as well as, their longitudinal evolution, in order to detect the disease onset.

In this paper, we focus on the problem of automatically detecting PD tremor from IMU data collected in-the-wild via a smartphone. Tremor detection in-the-wild, has received little attention from the research community, owing to the inherent difficulties of obtaining and properly annotating datasets in that setting. To this end, we introduce a new dataset of accelerometer recordings from both PD patients and healthy users, captured outside laboratory conditions and without any form of supervision or guidance, via a smartphone application developed in the context of [14].

Unlike other symptoms that are present all the time, tremor is of intermittent nature, that is, it may come and go unpredictably or, more formally, exhibit on and off periods. This problem is usually circumvented by recording the data acquisition sessions with a camera. The video is then used by medical experts to provide a fine-grained annotation of the on and off periods. However, this solution does not apply to data obtained unobtrusively in-the-wild, where observing the subjects throughout their daily lives is impossible. Hence, in that setting we must make do with the coarse label provided by the medical experts during the examination of the subject. Unfortunately, we cannot associate each IMU recording provided by a subject with this coarse tremor ground truth, as that would introduce severe label noise to our models that would prove devastating during training. Therefore, to mitigate this issue, we propose to address the problem at hand as a case of *Multiple-Instance Learning (MIL)*.

Multiple-Instance Learning [15] is a supervised learning scenario, where multiple instances or data points are grouped together to form sets, commonly referred to in MIL terminology as *bags* [16]. Each bag is associated with a single label that depends on the labels of the instances it contains according to some assumption. For example, the standard MIL assumption that we adopt in this paper, dictates that for a binary classification problem, a bag is considered positive if it contains at least one positive instance and negative if contains only negative instances. In our case, however, we are afforded with only an approximation of the true bag labels that is provided by an external oracle (be it the medical expert or the subject itself), who operates without any knowledge of the individual instance labels. For a detailed review of the different MIL assumptions, as well as the most popular algorithms and applications, we refer the reader to the survey of [16].

We can use the formalism of MIL to tackle the problem of tremor detection in-the-wild. The MIL framework naturally deals with the lack of fine-grained annotations (instance labels) and thus we can use it to adequately handle the particular nature of tremor: each subject can be represented as a bag of accelerometer signal segments and a tremor annotation that describes the whole bag. We propose a method to efficiently model the probability that a subject has tremor given their bag of acceleration segments, based on a recently proposed MIL method [17], that makes use of the attention mechanism [18] to identify key instances within a bag. The proposed method builds upon a previous work of ours [19], that showed very promising early results. In this paper, we extend that work by:

- i) Enriching the original dataset with 8 additional subjects for a total of 45 subjects.
- ii) Introducing an alternative approach that operates on the raw accelerometer values and outperforms the originally proposed spectrogram-based method.
- iii) Performing extensive experiments to confirm the potential of our method.
- iv) Publishing the dataset as open access data (available in <https://zenodo.org/record/3519213>.)

The rest of this paper is organized as follows. Section II discusses the most relevant work regarding in-the-wild tremor detection from IMU sensors. Section III presents the proposed tremor detection methodology. Section IV describes the dataset used in our experiments. Section V discusses the experimental setup and presents the results of our method along with those of other popular alternatives. Section VI contains a critical discussion of the proposed method. Finally, the paper concludes with section VII.

II. RELATED WORK

Parkinsonian tremor is an involuntary muscle contraction that typically exhibits at a frequency of 3-7 Hz. Its particular nature makes the use of inertial sensors, such as the accelerometers and gyroscopes embedded in modern phones, particularly appealing for developing data-driven tremor detection methods. Although many works have explored the use of such sensors for tremor detection, the research community has devoted little attention to developing algorithms that operate well outside laboratory conditions. Most approaches, such as [20], [21], are restricted to the home environment, while the evaluation of the symptom severity takes place at pre-defined moments during the day via self-administered tests, rather than occurring unobtrusively.

One of the works most related to ours is that of [22], in which the authors actually proposed a multiple-instance learning scheme to detect PD motor symptoms based on 5 body-worn accelerometers. Two subjects were tasked with wearing the sensors constantly for a period of four days while completing their regular daily living activities. The subjects were also asked to keep a journal of their medication intake and approximate time intervals on which symptoms occurred. After data collection, the accelerometer stream was segmented to windows of 6 seconds length and 1 second overlap, and several hand-crafted features were extracted from each window. All the window feature vectors pertaining to a specific time interval (of typical duration of 20 – 40 minutes) were used to create a bag whose label was defined by the symptom occurrence entry for that interval in the subject’s journal. The *Axis-Parallel Hyper-Rectangle (APR)* [23] algorithm was then trained using the acquired labeled bags from the first 8 hours of the first day of monitoring. Evaluation on the data recorded during the other days showed promising accuracy. However, the authors do not provide details about the class imbalance or the metrics affected by it (recall, specificity).

The more recent work of [24], extended the previous approach by using a dataset of 5 PD patients all of which exhibited tremor. Data collection took place under laboratory

conditions that resembled a home environment. In that setting, the subjects were free to perform any from a list of given activities, such as walking, writing or playing chess, while multiple cameras were used to provide detailed annotation regarding the tremor intensity at each moment. Standard hand-crafted features were extracted over 2-second windows with 1 second overlap. A window was considered tremorous if at least half contained a tremor episode as identified by the video. Consecutive window feature vectors were then pooled together into larger segments of length varying from 30 seconds to 10 minutes, to form a bag. Each such bag was labeled using two different methods: i) a bag was considered positive if it contained at least one positive window i.e. labeling according to the standard multiple-instance learning label assumption ii) a stratified method that considered the approximate percentage of tremor within a segment, quantized in 4 levels corresponding to 0-24%, 25-49%, 50-74% and 75-100%. The authors performed leave one subject out experiments with classical multiple-instance learning algorithms to show that performance rapidly deteriorates for the standard labeling approach as the segment length grows. Finally, they proposed a simple modification, applicable to all multiple-instance algorithms, that takes advantage of stratified labels so as to avoid the deterioration in performance caused by the decreasing label precision owing to the increase of the segment length.

While similar in spirit, our work differs from the previous approaches significantly. First of all, we use a large dataset of 45 subjects that contains both PD patients, with and without tremor, as well as completely healthy individuals. In addition, our dataset was collected unobtrusively and under completely unscripted and in-the-wild conditions. This means that the noise levels are expected to be significantly higher compared to data collected in lab or at home. Finally, contrary to other works, where fine-grained labels are available, we only have access to coarse subject-level labels, provided by experts. Therefore, the main contributions of this paper are:

- 1) A method for binary detection of Parkinsonian tremor from IMU data collected in-the-wild, that employs deep neural networks for feature extraction as well as a learnable pooling stage that can produce robust subject embeddings, leading to high classification performance.
- 2) A new, challenging dataset of IMU recordings, collected by a population of 45 PD and healthy subjects under completely unscripted and real-life conditions. The dataset is available online in <https://zenodo.org/record/3519213>.

III. MULTIPLE-INSTANCE TREMOR DETECTION

Supervised learning is the learning situation where we are provided with a set of instances $\mathbf{x}_i \in \mathbb{R}^N$ and their corresponding labels $y_i \in \mathcal{Y}$, and the goal is to infer a general mapping $f: \mathbb{R}^n \rightarrow \mathcal{Y}$. The label space \mathcal{Y} can be either \mathbb{R} (for regression problems) or \mathbb{Z} (for classification problems). The mapping f is usually chosen from a wide class of functions $\hat{f}(x; \theta)$ through an optimization procedure that minimizes some suitable cost function on the given set of instances, in order to find good values for the parameters θ . In the Multiple-Instance Learning setting, instead of individual instances, we are presented with

unordered sets of instances $X_j = \{\mathbf{x}_{j1}, \mathbf{x}_{j2}, \dots, \mathbf{x}_{jK_j}\}$, called *bags*, and their corresponding bag-level labels y_j . The goal in this scenario is to infer a mapping $f: 2^{\mathbb{R}^N} \rightarrow \mathcal{Y}$, where $2^{\mathbb{R}^N}$ denotes the power set of \mathbb{R}^N , that is to perform classification or regression on the bag level. In the rest of this work, we will assume that $\mathcal{Y} = \{0, 1\}$, since our focus is the case of binary classification of non-tremor (class 0) vs tremor (class 1). Hence, in our case the learned function f will map a given bag to the probability that it belongs to the positive class: $f(X; \theta) = p_{\text{model}}(y = 1|X) = 1 - p_{\text{model}}(y = 0|X)$.

Since we are dealing with unordered sets it is evident that the learned function f must be permutation invariant to the elements in a bag. The recent work of [25] provides a general strategy for modeling almost any permutation invariant function over a set X , as a sum decomposition of the form $f(X) = \rho(\sum_{\mathbf{x} \in X} \phi(\mathbf{x}))$, given suitable transformations ϕ, ρ . Thus, we can model the bag label probability as:

$$p_{\text{model}}(y = 1|X) = \rho\left(\sum_{\mathbf{x} \in X} \sigma(\phi(\mathbf{x}))\right) \quad (1)$$

where in our case:

- i) $\phi: \mathbb{R}^N \rightarrow \mathbb{R}^M$ independently maps each instance \mathbf{x}_i of X to a low-dimensional embedding of size M .
- ii) $\sigma: 2^{\mathbb{R}^M} \rightarrow \mathbb{R}^M$ is a weighted average of the instance embeddings that produces a fixed-length bag representation.
- iii) $\rho: \mathbb{R}^M \rightarrow [0, 1]$ transforms the pooled bag representation to the final bag label probability.

Equation 1 allows for increasingly flexible model designs. In particular, the function ϕ can be seen as performing feature extraction on each instance, while the function ρ is a classifier entity that outputs the final class estimation. In this work, we use neural networks to parameterize these two functions and adopt a learnable pooling scheme to compute the weight of each instance in the pooling function σ . More specifically, let $H = \{\mathbf{h}_1, \mathbf{h}_2, \dots, \mathbf{h}_K\} = \{\phi(\mathbf{x}_1), \phi(\mathbf{x}_2), \dots, \phi(\mathbf{x}_K)\}$ be a bag of K embeddings that results from the elementwise application of the embedding function ϕ to the initial bag X . According to equation 1, the function σ is defined as:

$$\mathbf{z} = \sigma(H) = \sum_{k=1}^K a_k \mathbf{h}_k \quad (2)$$

We can integrate learning of the weights a_k in the training procedure, by using a version of the attention mechanism [18], modified appropriately in [17] to work for MIL tasks, that takes the form:

$$a_k = \frac{\exp(\mathbf{w}^T \tanh(\mathbf{V}\mathbf{h}_k^T))}{\sum_{k=1}^K \exp(\mathbf{w}^T \tanh(\mathbf{V}\mathbf{h}_k^T))} \quad (3)$$

Computation of the quantities a_k is a highly non-linear procedure, since the value of each a_k depends both on the value of the relevant embedding \mathbf{h}_k , as well as the learnable parameters $\mathbf{w} \in \mathbb{R}^{L \times 1}$ and $\mathbf{V} \in \mathbb{R}^{L \times M}$, via a composition of non-linear functions. As we will see in section V, the construction of Equation 3 is capable of identifying and assigning large weights to key instances within a bag, allowing the final classifier stage (the function ρ) to perform efficient

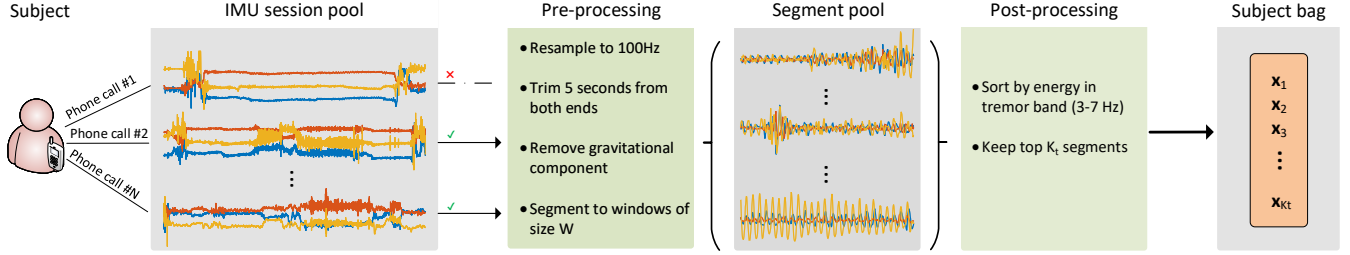


Fig. 1: Overview of the bag creation process. Each subject is assigned a bag of accelerometer signal segments captured during phone calls, and a single tremor label provided by experts.

bag classification. This allows us to identify which instances contributed the most to the model’s decision, thus adding a degree of interpretability to the method.

We propose to apply the attention-based multiple-instance framework described above to the problem of detecting Parkinsonian tremor from data collected in-the-wild. The rest of this section outlines the process of creating a bag for each subject using their contributed IMU data and the training procedure of our tremor detection model.

A. Bag creation

During data collection, each subject contributes one tri-axial accelerometer session for every phone call they make during their participation period. Each phone call may be of variable duration, which means that the recorded signals will be of variable length. However, the bag instances are assumed to be of a specific dimensionality ($\mathbf{x}_i \in \mathbb{R}^N$). To circumvent this issue, we resort to windowing each session into non-overlapping segments of length W samples. In doing so, we choose not to model possible intra-session dependencies between neighboring segments. However, based on our experimental results, this does not affect the method’s performance.

Let $S_i = \{\mathbf{w}_1, \mathbf{w}_2, \dots, \mathbf{w}_{n_i}\}$ be the result of performing segmentation on the i -th session of a subject, where $\mathbf{w}_j \in \mathbb{R}^{3 \times W}$ and n_i denotes the number of segments extracted from session i . Given the session segments, we apply a pre-filtering step, where only windows with energy above a threshold E_{\min} are kept. Sessions that end up with less than 2 segments after this step, are discarded altogether. The surviving segments across all sessions are collected in a large pool and sorted based on their energy in the band $[3, 7]$ Hz (the PD tremor band). Finally, the top K_t (a scalar hyperparameter, common to all subjects) segments are drawn from the sorted pool and are used to form the bag of the subject, which is of the form $X = \{\mathbf{x}_1, \mathbf{x}_2, \dots, \mathbf{x}_{K_t}\}$. A schematic overview of the bag creation procedure for a subject is given in Figure 1. For subjects that have less than K_t segments, we apply zero-padding to reach the desired bag length and implement a masking system that ignores these zero-padded instances during our computations.

B. Model training

Each extracted bag X is then associated with the available, expert-provided, tremor label y of the subject, to form a tuple

of the form (X, y) . The set of these tuples is the training set on which we will train our multiple-instance model.

In our previous work [19], the function ϕ operated on the frequency domain. In particular, we used a fully-connected neural network to perform feature extraction from the spectral representation of each instance. In other words, each instance was first transformed into its frequency representation and then fed into the network. In this work, we propose an approach in which the function ϕ operates on the time domain and uses a *Convolutional Neural Networks (CNN)* to extract features directly from the raw tri-axial acceleration signal. We do not employ a CNN directly on the spectrogram, because we are interested in high values in specific spectral coefficients (those corresponding to 3-7 Hz) and CNNs are by nature translation invariant. This means that a filter that has learnt to detect peaks would not be able to differentiate between a peak at 4 Hz and a peak at 20 Hz. Regarding the rest of the components, the pooling stage σ is implemented as a simple two-layer fully-connected network, while for the final classifier ρ we use multiple fully-connected layers. Details regarding the specific architecture choices of each stage are given in Section V.

The whole model, comprising the composition of ρ, σ, ϕ is trained end-to-end for E epochs using the cross-entropy loss:

$$\mathcal{L} = -\mathbb{E}_{X, y \sim \hat{p}_{data}} [y \log(p_{\text{model}}(y = 1|X)) + (1 - y)(1 - \log(p_{\text{model}}(y = 1|X)))] \quad (4)$$

where \hat{p}_{data} denotes the empirical data distribution defined by the available training data. Finally, when used for inference, the class probability estimate provided by the model is transformed into a class prediction using a threshold T .

IV. IN-THE-WILD DATA COLLECTION AND PRE-PROCESSING

A. Collection

We propose to collect in-the-wild IMU data through a mobile application developed in the context of [14]. The data collection application operates on the background and unobtrusively initiates recording of the accelerometer sensor whenever a phone call, either incoming or outgoing, is placed. The recording lasts at most for the first 75 seconds of the phone call, so as to avoid draining the battery. Each recording, consisting of the tri-axial accelerometer values, their timestamps and some metadata, is stored locally and transmitted

TABLE I: Demographic characteristics of the subjects in our dataset. For age, UPDRS scores, data contribution and relative energy, we report the average value and in parenthesis the standard deviation across the corresponding sub-population. UPDRS20 and UPDRS21 values refer to the sum of both hand scores. Relative energy refers to the ratio of energy in the tremor band (3-7 Hz) over the total energy of a segment.

	Healthy Controls	PD Patients	Total
Count	14	31	45
Age in years	55.4 (11.7)	62.1 (7.3)	60.0 (9.4)
Years diagnosed	-	6.3 (3.6)	-
UPDRS 16	0.07 (0.25)	1.09 (0.89)	-
UPDRS 20	0 (0)	1.19 (1.25)	-
UPDRS 21	0 (0)	0.96 (1.51)	-
Sum of UPDRS-III	2.28 (3.47)	19.7 (11.5)	-
No. of sessions	99.6 (151.3)	131.1 (166.2)	121.3 (162.4)
Session duration	30.4 (13.7)	33.8 (14.6)	32.9 (14.5)
Processed segments	441.0 (512.4)	576.8 (537.2)	534.6 (533.3)
Relative energy	0.35 (0.15)	0.38 (0.21)	0.37 (0.20)

wirelessly on a server, when the appropriate conditions, e.g. adequate battery levels, Wi-Fi access, etc., are met.

B. Pre-processing

Due to the wide variety of different recording devices expected during data collection, a common pre-processing step is designed and applied to all collected signals to ensure their homogeneity. First, problematic signals are discarded altogether. The rejection criteria for a signal are: i) its total duration is less than 20 seconds, ii) its estimated sampling frequency is below 50 Hz, iii) it contains extreme values ($> 100 m/s^2$), iv) it contains too many missing values. Signals that pass the rejection process are subsequently resampled to a sampling frequency of 100 Hz, through the use of a polyphase resampling step that involves linear interpolation, a downsampling step of appropriate ratio, a low-pass filter and an upsampling step, again, of appropriate ratio. A segment of 5 seconds is then removed from the start and the end of the sessions, so as to discard the moments when the user either picks up or hangs up the phone. In addition, the gravitational component of the acceleration signal is removed via a high-pass FIR filter of order 512 with a cutoff frequency of 1 Hz.

C. Annotation

To acquire tremor annotations for each subject, we resort to the *Unified Parkinson’s disease rating scale (UPDRS)* [26]. The UPDRS is the most commonly used scale used by physicians to quantify the severity of the various items in the PD symptomatology and keep track of the disease’s longitudinal progression. It includes a self-reported part (part II), where subjects themselves provide an estimation of their symptom severity during daily living, as well as a motor examination part (part III), where the attending physician examines the subject using a standardized set of motor tests, and provides a clinical evaluation of their status with respect to each symptom. Each symptom (corresponding to a specific UPDRS item) is given a score, generally between 0 and 4, with 0 signifying absence of symptom. Regarding tremor,

the relevant UPDRS items are: UPDRS16, the subject’s self-report for tremor at any body part, UPDRS20, the physician’s score for hand tremor at rest, and UPDRS21, the physician’s score for action or postural hand tremor. In reality, UPDRS20 contains separate sub-items concerning the existence of tremor in each body extremity separately. However, as our focus is on hand tremor, in the rest of this paper UPDRS20 will refer only to the hand items.

All UPDRS scores that belong to the motor examination part (UPDRS part III) were obtained by certified neurologists at three locations: the Department of Neurology of the Technical University of Dresden, Germany, the Department of Basic and Clinical Neuroscience of the King’s College Hospital, London and the Third Neurological Clinic of the Papanikolaou Hospital of Thessaloniki. All subjects in the dataset underwent a thorough neurological examination, strictly adhering to the protocol of a UPDRS motor examination, at the location corresponding to their country of residence.

Since our goal is to perform tremor detection, we use the binarized sum of the individual hand scores as the final target label. That is, if the sum of scores across hands is positive, we consider that the subject belongs to the positive class (has tremor). Accordingly, if the sum of hand scores is 0 we consider the subject to be of the negative class (no tremor). This leads to 3 potential sources of annotation, mainly the binary versions of UPDRS16, UPDRS20 and UPDRS21. However, one potential complication is that the UPDRS examination provides a clue as to the tremor severity only at the moment of the examination. This can be problematic since the examination could have coincided with an off period, and therefore no tremor would be observed by the doctor. In addition, a subject may have contributed too few data for the symptom to be observed or they could have tremor only on one hand and handle their device during phone calls with the other. Each such eventuality is a source of label noise that could severely affect the training of our algorithm. Hence, to overcome these issues we resort to an additional source of annotation that is produced by a group of signal processing experts after visually inspecting the contributed signals of each subject. A detailed account of how this annotation was produced is given in V.

V. EXPERIMENTAL EVALUATION

In this section, we conduct a series of experiments to evaluate our method with respect to the following aspects:

- Its efficacy in detecting tremorous episodes in-the-wild.
- Its dependence on the bag length.
- Its performance relative to popular alternatives.

For our experiments, we used a dataset of accelerometer recordings that was collected in-the-wild via smartphone-embedded IMU sensors. More specifically, multiple subjects, both PD patients and healthy controls, recruited by the medical experts participating in the study, downloaded the data collection Android application, described in section IV-A, and installed it on their personal smartphones. The typical contribution period of a subject ranged from a few weeks to several months, as they were free to uninstall the application

at any time. Therefore, each subject in the dataset contributed a different amount of recordings, that depended on both the number of phone calls they realized during the data collection period, as well as the duration of that period itself. In addition, we imposed a minimum requirement on the amount of data contributed from each participant in order for them to be considered. Specifically, subjects whose bag contained less than 30 segments in total after the session rejection step of section IV-B and the segment rejection step of section III-A, were not considered in our experiments. Ultimately, this led to a final dataset of 45 subjects. Additional details regarding the demographics of the subjects and their data contribution are given in Table I.

Each subject in the dataset underwent a full clinical evaluation, including a UPDRS assessment carried out by neurologists, at some point during their data contributing period. In addition, a group of 2 signal processing experts from our group used the subjects with the most extreme UPDRS scores to acquire a sense of how tremor manifests in acceleration signals. Then, the rest of the subjects were annotated by individually inspecting the raw accelerometer signal of each recording they had contributed as well as its spectrogram, and taking into account both the subject’s self-report and its clinical evaluation. During this process, a subject was labeled as tremorous if a tremorous episode could be detected in at least one of their contributed sessions upon visual inspection, in compliance with the standard MIL assumption [15]. The output of this process was used as an extra signal processing expert annotation.

We evaluated our approach using two experimental methodologies: a *Leave One Subject Out (LOSO)* scheme and a *Repeated k-Fold (RkF)* scheme. In the LOSO scheme, we use the data from all the subjects except one to train a model, evaluate the trained model on the left-out subject and repeat the process so that all subjects are used for evaluation once. In the RkF scheme, we split the subject group into k parts, use the data from the subjects belonging to the $k - 1$ parts to train a model and evaluate it on the subjects belonging to the other part. The process is repeated so that all parts are used once for evaluation and multiple repetitions of this procedure are conducted (hence, the “repeated” in its name) for different permutations of the subject group. In each repetition of both experimental schemes, we conducted multiple trials to account for the randomness inherent in the examined algorithms. We performed training using the signal processing experts annotations, as we consider them to be the most robust. Evaluation was performed using each of the available annotations, mainly UPDRS16, UPDRS20, UPDRS21 and signal processing expert (denoted SP-expert for short) annotations.

For computing the energy of a segment in the band of 3 – 7Hz (a step required during the bag creation phase) we used its frequency representation (computed according to Welch’s method for spectral density estimation, as described below) and summed the components that corresponded to that frequency band. We also used $E_{\min} = 0.15$ for discarding segments with low activity. For our deep multiple-instance approach, we used a window length W of 500 samples, i.e. 5 seconds given the common sampling frequency of 100

Hz. For the instance embedding function, ϕ , we examined 2 different approaches, the one proposed in [19] that operates on the frequency domain and the one proposed in this paper that operates on the time domain. The frequency domain approach, transforms each acceleration axis individually to the frequency domain using Welch’s method with a window size of 3 seconds and 75% overlap. Subsequently, the spectra across the 3 axes are summed and the coefficients that correspond to the frequency range $[0, 25]$ Hz are kept, thus leading to a vector of 76 elements. This frequency representation is then fed to a fully-connected network of multiple layers to acquire the instance embedding. On the contrary, the time domain approach operates directly on raw signal values and employs a CNN to extract features for each instance. In the following, we will refer to the former approach as *Deep-MIL-FC* and to the latter as *Deep-MIL-CNN*.

For both approaches, we resorted to standard network architectures that are used throughout the literature for classification problems. Specific details about each architecture are given in Table IV. Apart from the embedding function ϕ , we kept the rest of the model architecture identical. We used an embedding dimension, M , equal to 64. The attention pooling stage was modeled by two fully-connected layers that implemented Equation 3, with the attention dimension, L , set to 16. The values for the hyperparameters M , L were selected by experimentation on a small subset of the dataset. The final classifier stage, ρ , was also implemented as a fully-connected network with multiple layers (described in Table V). The whole model was trained end-to-end for E epochs using the Adam [27] optimizer with learning rate $\epsilon = 0.001$ and the suggested default values for the parameters β_1, β_2 . Learning rate decay was also applied during the last half of the training that exponentially reduced the learning rate at the beginning of each epoch by a factor of 0.9. The decision threshold, T , was set to 0.5. In total, the Deep-MIL-CNN model had 46627 trainable parameters and the Deep-MIL-FC model 65603.

We compared our method against 7 alternatives for solving MIL problems. More specifically, we employed a *Bag of Features (BoF)* [32] scheme for encoding a subject’s bag and then used an SVM with the chi-square kernel to train a classifier on the resulting bag encodings. We also examined the use of the more robust *Fisher Vector (FV)* [33] encoding scheme coupled with a linear SVM, similar in spirit to [31]. We also compared against the *Multiple Instance SVM (MI-SVM)* algorithm [30], an SVM variant whose formulation is modified so that it can solve multiple-instance problems. In addition, we evaluated against the models proposed by the authors of [28], who suggest a similar architecture to the methodology adopted in this paper. That is, a feature-extraction network that operates on each bag instance independently, followed by a pre-defined pooling operator, such as mean, max or log-sum-exp, and, ultimately, a linear transformation to the bag label probability. They propose 3 different models for producing the bag embedding: a fully-connected network followed by the pooling operator, a fully-connected network with deep supervision, where for each hidden layer a different bag pooling is produced and used for classification, and a fully-connected network with residual connections, where in each

TABLE II: Evaluation results for the LOSO experiment with bag length $K_t = 1500$. For each method we report the average and the standard deviation of its performance metrics across 10 independent LOSO trials. Notice that the implementation of MI-SVM that we use is fully deterministic, so there is no variance in its performance. Deep-MIL-FC was trained for $E = 1000$ epochs and Deep-MIL-CNN for $E = 50$ epochs. UPDRS annotations refer to binary versions of the physician-provided UPDRS scores.

Evaluation on	Model	Precision	Sensitivity	Specificity	F1-score
UPDRS16 (24 positive - 21 negative)	Simple-MIL	0.862 ± 0.047	0.362 ± 0.027	0.933 ± 0.023	0.522 ± 0.030
	MI-Net-Simple [28]	0.808 ± 0.052	0.442 ± 0.028	0.876 ± 0.044	0.586 ± 0.020
	MI-Net-DS [28]	0.759 ± 0.036	0.454 ± 0.012	0.833 ± 0.032	0.588 ± 0.012
	MI-Net-Res [28]	0.711 ± 0.034	0.458 ± 0.019	0.786 ± 0.032	0.579 ± 0.017
	BSN [29]	0.801 ± 0.054	0.425 ± 0.045	0.876 ± 0.049	0.570 ± 0.041
	Deep-MIL-FC [19]	0.799 ± 0.004	0.496 ± 0.013	0.857 ± 0.001	0.628 ± 0.010
	Deep-MIL-CNN (this paper)	0.780 ± 0.028	0.475 ± 0.038	0.848 ± 0.019	0.608 ± 0.033
	MI-SVM [30]	1.000 ± 0.000	0.250 ± 0.000	1.000 ± 0.000	0.400 ± 0.000
	BoF + SVM [31]	0.782 ± 0.098	0.208 ± 0.019	0.929 ± 0.038	0.340 ± 0.024
	FV + SVM [31]	0.597 ± 0.036	0.438 ± 0.057	0.662 ± 0.050	0.523 ± 0.036
UPDRS20 (17 positive - 28 negative)	Simple-MIL	0.734 ± 0.054	0.435 ± 0.029	0.904 ± 0.023	0.587 ± 0.029
	MI-Net-Simple [28]	0.620 ± 0.060	0.476 ± 0.018	0.818 ± 0.046	0.601 ± 0.016
	MI-Net-DS [28]	0.597 ± 0.014	0.506 ± 0.029	0.793 ± 0.014	0.617 ± 0.019
	MI-Net-Res [28]	0.568 ± 0.024	0.518 ± 0.024	0.761 ± 0.023	0.616 ± 0.018
	BSN [29]	0.551 ± 0.037	0.412 ± 0.037	0.793 ± 0.042	0.540 ± 0.027
	Deep-MIL-FC [19]	0.731 ± 0.006	0.641 ± 0.018	0.857 ± 0.001	0.733 ± 0.012
	Deep-MIL-CNN (this paper)	0.714 ± 0.048	0.612 ± 0.039	0.850 ± 0.031	0.711 ± 0.032
	MI-SVM [30]	0.667 ± 0.000	0.235 ± 0.000	0.929 ± 0.000	0.375 ± 0.000
	BoF + SVM [31]	0.725 ± 0.077	0.276 ± 0.046	0.936 ± 0.021	0.425 ± 0.056
	FV + SVM [31]	0.473 ± 0.033	0.488 ± 0.053	0.668 ± 0.051	0.560 ± 0.029
UPDRS21 (13 positive - 32 negative)	Simple-MIL	0.575 ± 0.034	0.446 ± 0.031	0.866 ± 0.014	0.588 ± 0.029
	MI-Net-Simple [28]	0.466 ± 0.045	0.469 ± 0.023	0.778 ± 0.041	0.585 ± 0.018
	MI-Net-DS [28]	0.458 ± 0.015	0.508 ± 0.038	0.756 ± 0.012	0.606 ± 0.019
	MI-Net-Res [28]	0.439 ± 0.022	0.523 ± 0.031	0.728 ± 0.020	0.608 ± 0.022
	BSN [29]	0.392 ± 0.026	0.385 ± 0.049	0.756 ± 0.036	0.507 ± 0.038
	Deep-MIL-FC [19]	0.597 ± 0.009	0.685 ± 0.023	0.812 ± 0.001	0.743 ± 0.014
	Deep-MIL-CNN (this paper)	0.576 ± 0.044	0.646 ± 0.051	0.806 ± 0.027	0.716 ± 0.037
	MI-SVM [30]	0.333 ± 0.000	0.154 ± 0.000	0.875 ± 0.000	0.262 ± 0.000
	BoF + SVM [31]	0.567 ± 0.078	0.285 ± 0.060	0.912 ± 0.019	0.430 ± 0.073
	FV + SVM [31]	0.411 ± 0.031	0.554 ± 0.058	0.675 ± 0.049	0.605 ± 0.030
SP-expert annotations (16 positive - 29 negative)	Simple-MIL	0.753 ± 0.044	0.475 ± 0.031	0.914 ± 0.017	0.625 ± 0.029
	MI-Net-Simple [28]	0.808 ± 0.052	0.662 ± 0.041	0.910 ± 0.032	0.765 ± 0.023
	MI-Net-DS [28]	0.799 ± 0.019	0.719 ± 0.042	0.900 ± 0.010	0.798 ± 0.026
	MI-Net-Res [28]	0.756 ± 0.029	0.731 ± 0.029	0.869 ± 0.021	0.794 ± 0.018
	BSN [29]	0.787 ± 0.062	0.625 ± 0.056	0.903 ± 0.037	0.737 ± 0.036
	Deep-MIL-FC [19]	0.933 ± 0.001	0.869 ± 0.019	0.966 ± 0.001	0.914 ± 0.011
	Deep-MIL-CNN (this paper)	0.987 ± 0.027	0.900 ± 0.057	0.993 ± 0.014	0.943 ± 0.034
	MI-SVM [30]	0.833 ± 0.000	0.312 ± 0.000	0.966 ± 0.000	0.472 ± 0.000
	BoF + SVM [31]	0.883 ± 0.084	0.356 ± 0.049	0.972 ± 0.021	0.519 ± 0.054
	FV + SVM [31]	0.580 ± 0.071	0.631 ± 0.059	0.741 ± 0.064	0.679 ± 0.043

hidden layer the pooling operator is applied on the sum of the current hidden representation with the hidden representation of the previous layer. Lastly, we compared with the approach of [29], that builds upon the MI-Net model to introduce a 2 stage approach: it first learns a bag similarity metric via a trained MI-Net model and it then uses it to derive a bag representation vector, based on the similarities of the given bag with a set of reference bags.

We denote the above models as *MI-Net-Simple*, *MI-Net-DS*, *MI-Net-Res* and *BSN* respectively. For each of these methods, we used max pooling as the pooling operator, because it was reported in both works to give consistent performance across different problems. Finally, as a very simple baseline, we also compared against a “naive” MIL algorithm (denoted as Simple-MIL in Table II), in which the bag label (i.e the subject label) was propagated to all the bag instances and a standard supervised model that classifies segments was trained.

The decision for the left-out subject was then computed as the average of the model’s predictions for all the instances in their bag.

For efficiency purposes, all the algorithms used for comparison (including the simple-MIL approach, which used the exact same architecture as the Deep-MIL-FC algorithm) operated on the frequency domain, that is, they accepted as input bags of spectrograms, computed in the same way as in the frequency-based MIL approach. For the BoF encoding we used a codebook of size 128, while for the FV encoding we used a GMM with 64 modes. In both cases, the base C hyperparameter of the SVM was set to 1 and then balanced according to the class prior. For the MI-SVM approach, we used a linear kernel with C equal to 100, after experimenting with as small subset of the data. Finally, for comparing against the MI-Net variants, we used an underlying network architecture as close as possible to the Deep-MIL-FC algorithm.

Table II presents the results of the LOSO experiment for

TABLE III: Evaluation results for the Repeated k -Fold experiment with $k = 5$ and bag length $K_t = 1500$. For each method we report the average and the standard deviation of its performance metrics across 10 repetitions (and 5 random trials per repetition) of the 5-fold experiment.

Evaluation on	Model	Precision	Sensitivity	Specificity	F1-score
UPDRS16 (24 positive - 21 negative)	Simple-MIL	0.846 \pm 0.017	0.356 \pm 0.006	0.923 \pm 0.010	0.514 \pm 0.006
	MI-Net-Simple [28]	0.827 \pm 0.016	0.470 \pm 0.010	0.888 \pm 0.010	0.615 \pm 0.011
	MI-Net-DS [28]	0.754 \pm 0.006	0.479 \pm 0.004	0.821 \pm 0.006	0.605 \pm 0.003
	MI-Net-Res [28]	0.751 \pm 0.012	0.478 \pm 0.011	0.819 \pm 0.009	0.604 \pm 0.010
	BSN [29]	0.802 \pm 0.021	0.426 \pm 0.013	0.880 \pm 0.014	0.574 \pm 0.013
	Deep-MIL-FC [19]	0.803 \pm 0.007	0.474 \pm 0.003	0.867 \pm 0.006	0.613 \pm 0.003
	Deep-MIL-CNN (this paper)	0.778 \pm 0.012	0.449 \pm 0.009	0.853 \pm 0.010	0.588 \pm 0.008
	BoF + SVM [31]	0.754 \pm 0.027	0.247 \pm 0.007	0.908 \pm 0.013	0.388 \pm 0.008
	FV + SVM [31]	0.627 \pm 0.011	0.460 \pm 0.011	0.688 \pm 0.014	0.551 \pm 0.008
UPDRS20 (17 positive - 28 negative)	Simple-MIL	0.759 \pm 0.015	0.457 \pm 0.008	0.856 \pm 0.008	0.595 \pm 0.009
	MI-Net-Simple [28]	0.617 \pm 0.010	0.495 \pm 0.007	0.814 \pm 0.005	0.616 \pm 0.007
	MI-Net-DS [28]	0.554 \pm 0.004	0.498 \pm 0.003	0.757 \pm 0.005	0.601 \pm 0.002
	MI-Net-Res [28]	0.559 \pm 0.004	0.502 \pm 0.006	0.759 \pm 0.005	0.605 \pm 0.004
	BSN [29]	0.564 \pm 0.008	0.422 \pm 0.007	0.801 \pm 0.009	0.553 \pm 0.004
	Deep-MIL-FC [19]	0.719 \pm 0.006	0.600 \pm 0.004	0.858 \pm 0.004	0.706 \pm 0.003
	Deep-MIL-CNN (this paper)	0.723 \pm 0.012	0.589 \pm 0.004	0.863 \pm 0.009	0.700 \pm 0.002
	BoF + SVM [31]	0.682 \pm 0.019	0.315 \pm 0.013	0.911 \pm 0.007	0.468 \pm 0.015
	FV + SVM [31]	0.512 \pm 0.013	0.529 \pm 0.004	0.693 \pm 0.016	0.600 \pm 0.006
UPDRS21 (13 positive - 32 negative)	Simple-MIL	0.542 \pm 0.015	0.456 \pm 0.009	0.856 \pm 0.008	0.595 \pm 0.009
	MI-Net-Simple [28]	0.471 \pm 0.010	0.494 \pm 0.009	0.774 \pm 0.005	0.603 \pm 0.008
	MI-Net-DS [28]	0.423 \pm 0.003	0.497 \pm 0.004	0.725 \pm 0.004	0.590 \pm 0.002
	MI-Net-Res [28]	0.428 \pm 0.004	0.503 \pm 0.008	0.727 \pm 0.004	0.595 \pm 0.005
	BSN [29]	0.407 \pm 0.005	0.398 \pm 0.009	0.764 \pm 0.008	0.524 \pm 0.006
	Deep-MIL-FC [19]	0.578 \pm 0.005	0.631 \pm 0.005	0.813 \pm 0.004	0.710 \pm 0.003
	Deep-MIL-CNN (this paper)	0.579 \pm 0.009	0.617 \pm 0.006	0.818 \pm 0.008	0.703 \pm 0.003
	BoF + SVM [31]	0.555 \pm 0.019	0.335 \pm 0.017	0.891 \pm 0.006	0.487 \pm 0.018
	FV + SVM [31]	0.425 \pm 0.011	0.575 \pm 0.011	0.684 \pm 0.013	0.625 \pm 0.009
SP-expert annotations (16 positive - 29 negative)	Simple-MIL	0.766 \pm 0.017	0.528 \pm 0.005	0.920 \pm 0.008	0.671 \pm 0.004
	MI-Net-Simple [28]	0.820 \pm 0.006	0.699 \pm 0.005	0.915 \pm 0.003	0.792 \pm 0.004
	MI-Net-DS [28]	0.744 \pm 0.003	0.710 \pm 0.008	0.866 \pm 0.002	0.780 \pm 0.005
	MI-Net-Res [28]	0.754 \pm 0.007	0.720 \pm 0.014	0.870 \pm 0.004	0.788 \pm 0.009
	BSN [29]	0.787 \pm 0.020	0.626 \pm 0.005	0.906 \pm 0.011	0.741 \pm 0.005
	Deep-MIL-FC [19]	0.913 \pm 0.003	0.809 \pm 0.006	0.957 \pm 0.002	0.877 \pm 0.003
	Deep-MIL-CNN (this paper)	0.955 \pm 0.012	0.828 \pm 0.024	0.979 \pm 0.006	0.897 \pm 0.015
	BoF + SVM [31]	0.812 \pm 0.021	0.399 \pm 0.016	0.949 \pm 0.006	0.561 \pm 0.016
	FV + SVM [31]	0.722 \pm 0.017	0.684 \pm 0.008	0.770 \pm 0.016	0.724 \pm 0.009

TABLE IV: The architectures used for the embedding function ϕ . k denotes the kernel size, f the number of filters in the convolutional layers and M the final embedding dimension.

	Fully-connected	CNN
Input \mathbf{x}_k	1×76 spectrogram	3×500 raw acceleration
Layer 1	Dense $76 \rightarrow 256$ Leaky-ReLU ($\alpha = 0.2$) Dropout $p = 0.5$	Conv1D $k = 8, f = 32$ Leaky-ReLU ($\alpha = 0.2$) MaxPool $k = 2$
Layer 2	Dense $256 \rightarrow 128$ Leaky-ReLU ($\alpha = 0.2$) Dropout $p = 0.5$	Conv1D $k = 8, f = 32$ Leaky-ReLU ($\alpha = 0.2$) MaxPool $k = 2$
Layer 3	Dense $128 \rightarrow M$	Conv1D $k = 16, f = 16$ Leaky-ReLU ($\alpha = 0.2$) MaxPool $k = 2$
Layer 4		Conv1D $k = 16, f = 16$ Leaky-ReLU ($\alpha = 0.2$) MaxPool $k = 2$
Layer 5		Flatten Dense $320 \rightarrow M$
Output	$\mathbf{h}_k \in \mathcal{R}^M$	$\mathbf{h}_k \in \mathcal{R}^M$

our approach, as well as the alternative algorithms of the

TABLE V: Architecture of the final classifier ρ . M denotes the output dimension of the instance embedding function, ϕ .

Final classifier stage	
Input	$\mathbf{z} \in \mathcal{R}^M$ (see Equation 2)
Layer 1	Dense $M \rightarrow 32$ Leaky-ReLU ($\alpha = 0.2$) Dropout $p = 0.2$
Layer 2	Dense $32 \rightarrow 16$ Leaky-ReLU ($\alpha = 0.2$) Dropout $p = 0.2$
Layer 3	Dense $16 \rightarrow 2$ 2-way softmax
Output	$p(y X)$

previous paragraph for each available evaluation scheme. Table III presents the respective results for the RkF experiment. We can see that the attention-based models outperform the alternatives under almost all evaluation schemes. Specifically, when evaluation is performed on the signal processing expert labels, which can be considered as the most correct, our approach outperforms the alternatives by a significant margin.

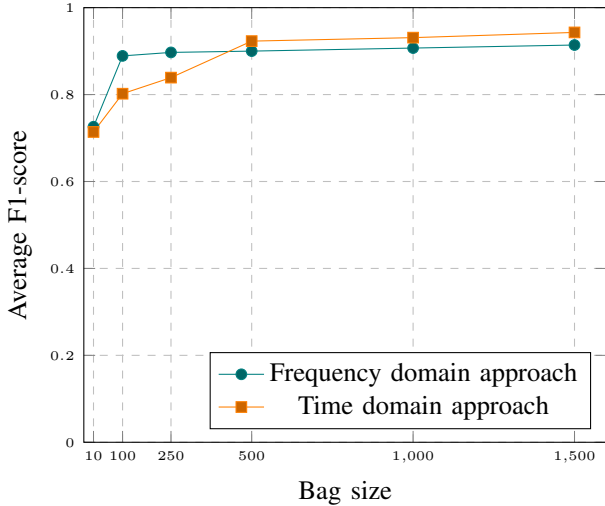


Fig. 2: Model performance (measured by the average F1-score across 10 LOSO trials) as a function of the bag size

Overall, the Deep-MIL-CNN model achieves the best performance suggesting that it is feasible to obtain good performance by training CNN feature extractors from scratch under the weakly-labeled scenario of multiple-instance learning. The observed gap in performance between the signal processing expert annotations and the medical expert ones, may appear large but the observed discrepancy can be attributed to the occurrence of label noise, the causes of which are discussed in the last paragraph of Section IV-C.

We also examine how different bag size values affect the classification performance. To this end we repeat the same experiment as above while varying the bag size. The change in performance as a function of the bag size K_t can be seen in Figure 2. In general, we can see that reasonable performance can be achieved with as little as 100 instances per bag. Moreover, it is interesting to notice that at the low bag size regime, the frequency domain approach achieves the best performance. This can be explained by the fact that CNNs require a large amount of data to be trained efficiently. Thus, as the bag size increases, more data are presented to the CNN and so the time domain approach catches up and finally outperforms the frequency-based approach.

Finally, we wish to evaluate the ability of the attention-based model to discover key instances within a bag. To that end, we visualize the 2 instances with the highest α_k and the 2 instances with the lowest α_k , as identified by the Deep-MIL-CNN model for a tremorous subject. As we can see in Figure 3, the model correctly assigns large weights to instances that contain tremorous episodes (sinusoidal components of $\approx 7Hz$) and low weights to instances without such patterns. This corroborates our hope that throughout its training, the model learns to discover tremor-related patterns in large sets of heterogeneous (with respect to the class label) instances, without being explicitly presented with such patterns, as in traditional supervised learning.

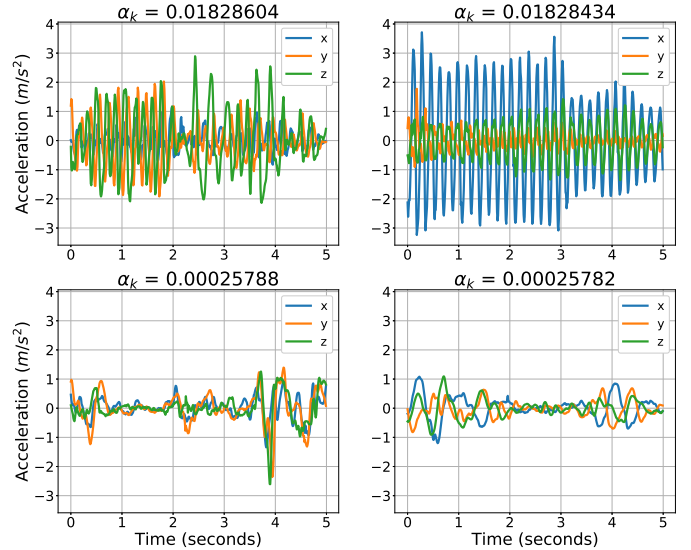


Fig. 3: Visualization of the top-2 and bottom-2 instances and their corresponding α_k coefficients, as identified by the CNN-based model for a tremorous subject. TOP ROW: The 2 instances with the largest α_k for the given subject. BOTTOM ROW: The 2 instances with the lowest α_k for the given subject.

VI. DISCUSSION

In general, we can say that the proposed method exhibits quite high classification performance and clearly outperforms the alternative methods. One explanation for this, is that the attention-based pooling scheme can accurately identify the positive instances within a bag. In problems where the data collection takes place in-the-wild and the targeted symptom is of intermittent nature, the number of positive instances within a bag can be very small. Thus, their contribution to the bag representation may be lost when performing frequency-based pooling (as in BoW or FV encoding) or mean pooling. On the contrary, the positive instances in the case of a well-trained attention-based pooling scheme will receive high weight, thus contributing significantly to the final bag representation. Combining the attention mechanism to a robust CNN feature extractor can, therefore, lead to the very good detection results we report. As a final note on this, we conjecture that the max pooling operator should perform equally well, since, in theory, it is insensitive to the small number of positive instances. However, we can see in the experimental results that this is not the case, suggesting that the attention-based pooling is more suitable for the training process.

However, in a real world deployment, the method would face a series of challenges, owing to the particular nature of tremor and the consequently problematic labeling mechanism. First of all, for evaluation purposes in such a scenario, any predictions made by the model would be compared against the opinions of the medical experts. If these opinions are expressed in terms of a single UPDRS evaluation, the performance of the algorithm will be underestimated, since, as we saw in Section IV-C, a single UPDRS examination is prone to producing erroneous labels, due to the tremor’s intermittence. Hence, some of the model’s predictions, while in fact correct,

would be perceived as wrong. A possible countermeasure to this, would be for the medical experts to re-evaluate these “false positive” predictions. In such a scenario, the number of subjects who will “waist” such a trip to the doctor, is expected to be very low, since the specificity of the model, as estimated by our experiments, is very high ($> 99\%$). High specificity is a very desirable property for an algorithm that operates as a warning system within a mobile phone environment and therefore aims for unobtrusiveness, because, in such use cases, a high false-positive rate is considered to be more detrimental than a high false-negative rate.

A different kind of problem appears when a subject has tremor in only one hand, but uses the unaffected hand to answer their phone calls. In such cases, we cannot hope to make a successful prediction, since all the data contributed by the subject will not contain tremorous episodes. Yet, according to the medical experts, the subject will belong to the positive class. Thus, this would unavoidably result in a false negative prediction. This is also true for cases where the subject makes a call with a bluetooth set, as in the current version of the data collection app we do not record whether bluetooth was used during the call and therefore cannot filter it out.

Another point of concern, stems from the dataset itself. As we can see in Table I, the ratio of Healthy controls over PD patients in our dataset (14 Healthy and 31 PD), is very different from the expected ratio in the general population (about 1% of the population above 60 years old). This is a result of the subject recruitment process, conducted by the medical experts participating in the study. In future work, we plan to re-evaluate our method on a larger dataset with many more subjects, so as to mitigate this concern.

A limitation of a more technical nature stems from the fact that the decision boundaries of the trained models tend to be very sharp, with the predicted class probabilities being biased towards very close to 0 or very close 1. This has the unfortunate side-effect that the output of a model cannot also serve as a confidence level of its prediction (which would be possible if the model did output probabilities around 0.5). One solution to this issue, that we consider as a step for future work, would be to train an ensemble of models, for example 10, and use the average class probabilities of all the models in the ensemble, as the final tremor probability for a subject.

Finally, in its current form, the proposed method operates on accelerometer signals captured only during phone call events. However, the overall idea is not limited to this data capturing approach and could just as well be applied to IMU data captured during more general interactions of the user with their phone, for instance from when the user is typing on the virtual keyboard of the device. Extending the current approach to work in such cases, is another direction for future work.

VII. CONCLUSION

We presented a method for performing binary tremor detection from accelerometer data obtained in-the-wild, in which each subject is represented by a bag of acceleration signal segments and a single tremor label. A deep multiple-instance learning approach that combined feature extraction and a

pooling scheme inspired by the attention mechanism, was used, in order to identify the key segments within each bag. The extensive experiments performed on a dataset of 45 subjects, indicate that the proposed method can indeed identify such instances and, therefore, successfully handle the in-the-wild setting of the recorded signals. Moreover, our method can be trained efficiently using only the coarse subject-level annotations available, thus efficiently handling the problem of weak supervision. Finally, it leads to dramatically improved performance over the examined alternatives.

ACKNOWLEDGMENT

The work leading to these results received funding from the EU Commission under Grant Agreement No. 690494 (<http://www.i-prognosis.eu>, H2020). Data collection was approved by the Institution’s Ethical Review Board and all participating subjects provided electronic consent.

REFERENCES

- [1] J. Jankovic, “Parkinson’s disease: clinical features and diagnosis,” *Journal of Neurology, Neurosurgery & Psychiatry*, vol. 79, no. 4, pp. 368–376, 2008.
- [2] F. L. Pagan, “Improving outcomes through early diagnosis of parkinson’s disease,” *American Journal of Managed Care*, vol. 18, no. 7, p. S176, 2012.
- [3] J. R. Orozco-Arroyave *et al.*, “Voiced/unvoiced transitions in speech as a potential bio-marker to detect parkinson’s disease,” in *Sixteenth Annual Conference of the International Speech Communication Association*, 2015.
- [4] A. Tsanas *et al.*, “Novel speech signal processing algorithms for high-accuracy classification of parkinson’s disease,” *IEEE Transactions on Biomedical Engineering*, vol. 59, no. 5, pp. 1264–1271, May 2012.
- [5] H. Gunduz, “Deep learning-based parkinsons disease classification using vocal feature sets,” *IEEE Access*, vol. 7, pp. 115 540–115 551, 2019.
- [6] L. Giancardo *et al.*, “Computer keyboard interaction as an indicator of early parkinsons disease,” *Scientific reports*, vol. 6, p. 34468, 2016.
- [7] D. Iakovakis *et al.*, “Touchscreen typing-pattern analysis for detecting fine motor skills decline in early-stage parkinsons disease,” *Scientific Reports*, vol. 8, 12 2018.
- [8] C. R. Pereira *et al.*, “Deep learning-aided parkinson’s disease diagnosis from handwritten dynamics,” in *2016 29th SIBGRAP Conference on Graphics, Patterns and Images (SIBGRAP)*, Oct 2016, pp. 340–346.
- [9] C. Caramia *et al.*, “Imu-based classification of parkinson’s disease from gait: A sensitivity analysis on sensor location and feature selection,” *IEEE Journal of Biomedical and Health Informatics*, vol. 22, no. 6, pp. 1765–1774, Nov 2018.
- [10] L. Ai *et al.*, “Classification of parkinsonian and essential tremor using empirical mode decomposition and support vector machine,” *Digit. Signal Process.*, vol. 21, no. 4, pp. 543–550, July 2011.
- [11] J. A. Gallego *et al.*, “Real-time estimation of pathological tremor parameters from gyroscope data,” *Sensors*, vol. 10, no. 3, pp. 2129–2149, 2010.
- [12] H. Dai *et al.*, “Quantitative assessment of parkinsonian tremor based on an inertial measurement unit,” *Sensors*, vol. 15, no. 10, pp. 25 055–25 071, 2015.
- [13] J.-F. Daneault *et al.*, “Using a smart phone as a standalone platform for detection and monitoring of pathological tremors,” *Frontiers in human neuroscience*, vol. 6, p. 357, 12 2012.
- [14] *i-PROGNOSIS: Towards an early detection of Parkinson’s disease via a smartphone application*. Zenodo, Sept. 2017.
- [15] T. G. Dietterich *et al.*, “Solving the multiple instance problem with axis-parallel rectangles,” *Artificial intelligence*, vol. 89, no. 1-2, pp. 31–71, 1997.
- [16] M.-A. Carbonneau *et al.*, “Multiple instance learning: A survey of problem characteristics and applications,” *Pattern Recognition*, vol. 77, pp. 329–353, 2018.
- [17] M. Ilse, J. Tomczak, and M. Welling, “Attention-based deep multiple instance learning,” in *Proceedings of the 35th International Conference on Machine Learning*, 10–15 Jul 2018, pp. 2127–2136.

- [18] A. Vaswani *et al.*, “Attention is all you need,” in *Advances in Neural Information Processing Systems 30*, 2017, pp. 5998–6008.
- [19] A. Papadopoulos *et al.*, “Multiple-instance learning for in-the-wild parkinsonian tremor detection,” in *41th Annual International Conference of the IEEE Engineering in Medicine and Biology Society (EMBC)*. IEEE, 2019.
- [20] S. Arora *et al.*, “High accuracy discrimination of parkinson’s disease participants from healthy controls using smartphones,” in *2014 IEEE International Conference on Acoustics, Speech and Signal Processing (ICASSP)*. IEEE, 2014, pp. 3641–3644.
- [21] S. Arora *et al.*, “Detecting and monitoring the symptoms of parkinson’s disease using smartphones: a pilot study,” *Parkinsonism & related disorders*, vol. 21, no. 6, pp. 650–653, 2015.
- [22] S. Das *et al.*, “Detecting parkinsons’ symptoms in uncontrolled home environments: A multiple instance learning approach,” in *2012 Annual International Conference of the IEEE Engineering in Medicine and Biology Society*. IEEE, 2012, pp. 3688–3691.
- [23] T. G. Dietterich *et al.*, “Solving the multiple instance problem with axis-parallel rectangles,” *Artificial intelligence*, vol. 89, no. 1-2, pp. 31–71, 1997.
- [24] A. Zhang *et al.*, “Weakly-supervised learning for parkinson’s disease tremor detection,” in *Engineering in Medicine and Biology Society (EMBC), 2017 39th Annual International Conference of the IEEE*. IEEE, 2017, pp. 143–147.
- [25] M. Zaheer *et al.*, “Deep sets,” in *Advances in Neural Information Processing Systems 30*, 2017, pp. 3391–3401.
- [26] S. Fahn *et al.*, “Recent developments in parkinson’s disease,” *Annals of Neurology*, vol. 22, no. 5, pp. 672–672, 1987.
- [27] D. P. Kingma and J. Ba, “Adam: A method for stochastic optimization,” *arXiv preprint arXiv:1412.6980*, 2014.
- [28] X. Wang *et al.*, “Revisiting multiple instance neural networks,” *Pattern Recognition*, vol. 74, pp. 15–24, 2018.
- [29] X. Wang *et al.*, “Bag similarity network for deep multi-instance learning,” *Information Sciences*, vol. 504, pp. 578–588, 2019.
- [30] S. Andrews *et al.*, “Support vector machines for multiple-instance learning,” in *Advances in neural information processing systems*, 2003, pp. 577–584.
- [31] X.-S. Wei *et al.*, “Scalable algorithms for multi-instance learning,” *IEEE transactions on neural networks and learning systems*, vol. 28, no. 4, pp. 975–987, 2016.
- [32] G. Csurka *et al.*, “Visual categorization with bags of keypoints,” in *Workshop on statistical learning in computer vision, ECCV*, vol. 1, no. 1-22. Prague, 2004, pp. 1–2.
- [33] J. Sánchez *et al.*, “Image classification with the fisher vector: Theory and practice,” *International journal of computer vision*, vol. 105, no. 3, pp. 222–245, 2013.